Self-assembled nanospheres mediate phototherapy and deliver CpG oligodeoxynucleotides to enhance cancer immunotherapy of breast cancer and melanoma

Guohui Yu [a,b,1], Fan Dong [a,1], Wenshu Ge [a,1], Lisha Sun [a], Ludan Zhang [a], Lintian Yuan [a], Ningyu Li [a], Hao Dai [a], Lei Shi [b,*], Yuguang Wang [a,*]

[a] Center of Digital Dentistry/Department of Prosthodontics, National Center of Stomatology, National Clinical Research Center for Oral Diseases, National Engineering Laboratory for Digital and Material Technology of Stomatology, Beijing Key Laboratory of Digital Stomatology, NHC Research Center of Engineering and Technology for Computerized Dentistry , Department of General Dentistry II, Central Laboratory, Peking University School and Hospital of Stomatology, Beijing 100081, China
[b] State Key Laboratory of Experimental Hematology, The Province and Ministry Co-sponsored Collaborative Innovation Center for Medical Epigenetics, Key Laboratory of Breast Cancer Prevention and Therapy (Ministry of Education), Department of Biochemistry and Molecular Biology, School of Basic Medical Sciences, Tianjin Medical University, Tianjin 300070, China

A R T I C L E   I N F O

A B S T R A C T

In the tumor microenvironment (TME) in certain cancer patients, the lack of tumor-associated antigens (TAAs) and low antigen presentation ability of antigen-presenting cells (APCs) limit the systemic immune effect of immune checkpoint blockade (ICB) therapy, which fails to elicit a persistent immune response. In this study, we used an important immune adjuvant (CpG ODN) and a photosensitizer (ICG) with 808 nm laser irradiation to trigger photodynamic and photothermal responses to synthesize intertwining DNA-photosensitizer nanosphere (iDP-NS) that can resolve the aforementioned shortcomings of current therapies and, together with programmed cell death-ligand 1 (PD-L1) treatment, convert uninflamed "cold" tumors into "hot" tumors. Hybrid nanosphere-mediated dual-modality photothermal/photodynamic therapy can be used to release TAAs and deliver immunostimulatory CpG ODNs to dendritic cells. In this approach, enhanced antigen presentation and immune checkpoint blockade therapy synergistically re-initiate toxic T cell activity and amplify immune effects, which can produce a powerful immune response and eliminate tumors in breast cancer and melanoma animal models. Notably, we proved that iDP-NSs mediated photo-immune response combined with ICB therapy can effectively trigger long immune memory to inhibit tumor recurrence and metastasis in 4T1 postoperative model.

© 2022 Published by Elsevier Ltd.

Introduction

Tumor immunotherapy is an important cancer treatment that stimulates or modulates the immune system to improve the intrinsic response of the host to tumors. These therapies include immune checkpoint blockade (ICB), cancer vaccines, adoptive T cell immunotherapy, etc [1–4]. Among these treatments, immune checkpoint blockade (ICB) has achieved great clinical success in recent years [5–7]. However, the lack of tumor-associated antigens (TAAs) in the tumor microenvironment (TME) and the low antigen presentation ability of antigen-presenting cells (APCs) limit the

duration of ICB effects [8–10]. Therefore, therapeutic strategies for enhancing the curative effect of ICB are of great research significance and clinical value. Related studies have demonstrated that functional phototherapeutic (photothermal/photodynamic therapy, PTT/PDT) nanoplatforms can induce cancer cell apoptosis and necrosis and release tumor cell debris, including TAAs [11–16]. In addition, the immune adjuvant CpG can activate APCs (such as dendritic cells (DCs), macrophages, and B cells) by triggering the Toll-like receptor 9 (TLR 9) pathway to further promote maturation of DCs and effectively enhance the effect of ICB. Recent studies have shown that immunogenic phototherapy combined with immune adjuvants can further improve the therapeutic effect of ICB in the tumor micro-environment [17–19]. The use of CpG oligodeoxynucleotides (CpG-ODNs) in combination with phototherapy can synergistically activate

---

* Corresponding authors.
[1] These authors contributed equally to this work.

the immune system and enhance tumor immunotherapy. In recent years , co-delivery strategies of various drugs have greatly facilitated the treatment and application of drugs. The rapid development of the field of drug therapy is inseparable from the continuous pursuit of advanced delivery technologies and strategies. However, new functions inevitably bring new challenges, such as the issues of protein and peptide stability, nucleic acid delivery efficiency into cells, proliferation of living cells and so on. To meet these challenges, drug delivery strategies must continue to innovate, many problems need to be solved with respect to the co-delivery strategy of immunoadjuvant and immunogenic phototherapeutic agents. A few decades ago, small-molecule drugs were the most important therapeutic drugs, but their delivery largely depends on the physicochemical properties of their structures, which severely affects the bioavailability of drugs, thus improving the solubility of drugs and controlling their release, optimizing their activities and improving their pharmacokinetics are the first delivery issues to be addressed.

In recent years, the applications of nano metal-organic frameworks (nMOFs) formed by metal ions and photosensitizers *via* coordinated bond to immunogenic phototherapy have been well documented. Loading functional molecules (*e.g.*, nucleic acids, proteins, and nucleic and acidic proteins) on the basis of MOFs porous structure or electrostatic adsorption can satisfy the requirements of the two aforementioned therapeutic strategies. It is still difficult to integrate photosensitizers and immune adjuvants in a one-step synthetic process [20–22]. Reducing the complexity of material synthesis processes and increasing the functionality of materials remain challenges in the field of nanomaterials based on nucleic acid and photosensitizers. Recently, Li et al. reported a simple method for triggering nanoparticle self-assembly, in this strategy, interactions between molecules are coordinated through metal ions, which assemble them into one system [23]. Due to its flexible component pattern and good biodegradability, this platform has attracted the attention of researchers. Based on this rationale used to self-assemble nanoparticles, we speculate that metal ions, photosensitizers and immune adjuvants can be combined to synthesize a new DNA-photosensitizer co-delivery system through coordinated self-assembly.

Herein, we used Fe^{II} ions to assemble CpG oligonucleotides (CpG ODNs) and the photosensitizer indocyanine green (ICG) into intertwining DNA-photosensitizer nanospheres (iDP-NSs) as nano-vaccines for efficient co-delivery and immunomodulation towards the tumor microenvironment. These carrier-free nanospheres release TAAs through ICG-mediated immunogenic phototherapy and enhance the delivery efficiency of CpG to DCs. In the tumor microenvironment, the enhanced antigen-presenting ability of the iDP-NSs significantly improve the therapeutic effect of ICB, and the powerful immune effect resultfully overcame tumor recurrence and metastasis (Scheme 1).

Materials and methods

All experimental materials and methods are included in the Supporting Information.

Results and discussion

Preparation and characterization of iDP-NS

A CpG ODN is an important immune adjuvant that activates TLR9 receptors in antigen-presenting cells (APCs). Indocyanine green (ICG) is a NIR dye with 808 nm laser irradiation that can trigger extremely powerful photodynamic and photothermal effects. Most importantly, the aforementioned small molecules have good biocompatibility, which is beneficial for their application in clinical treatment. In this study, we used Fe^{II} to coordinate CpG ODN and ICG through a self-assembly method to synthesize iDP-NSs at 95 °C for 1–3 h. After washing and centrifugation, the final nanospheres were obtained (Fig. S1 and 1 e). As shown in Fig. 1a, scanning electron microscopy (SEM) shows that the iDP-NSs maintain a regular 3D structure and uniform size. The lack of lattice fringes and diffraction contrast in the high-resolution TEM (HRTEM) image and fast Fourier transform (FFT) patterns of the iDP-NSs indicated that iDP-NSs have amorphous nature (Fig. 1b&1b inset). Dynamic light scattering (DLS) measurements showed number-average diameters of 150–200 nm for the iDP-NSs (Fig. 1c). Zeta potential was determined to investigate the surface charge of the iDP-NSs. XRD studies revealed that iDP-NSs are isostructural compared to previously reported Fe-DNA nanospheres (Fig. S3) [24]. Compared with Fe-DNA nanospheres, the iDP-NSs showed a change in potential, indicating
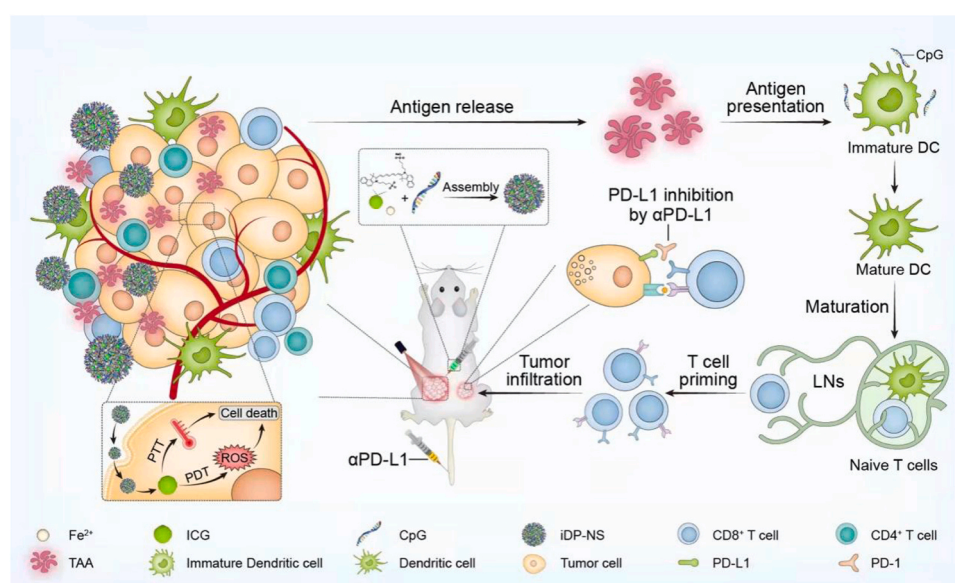
Scheme 1. Schematic diagram of the structure and preparation process of iDP-NS and their application to mediate phototherapy and deliver CpG oligodeoxynucleotides to enhance cancer immunotherapy of breast cancer and melanoma.

(a) (b) (c) (d)

(e) (f) (g)

(h)

(i) (j) (k)

(l) (m) (n)
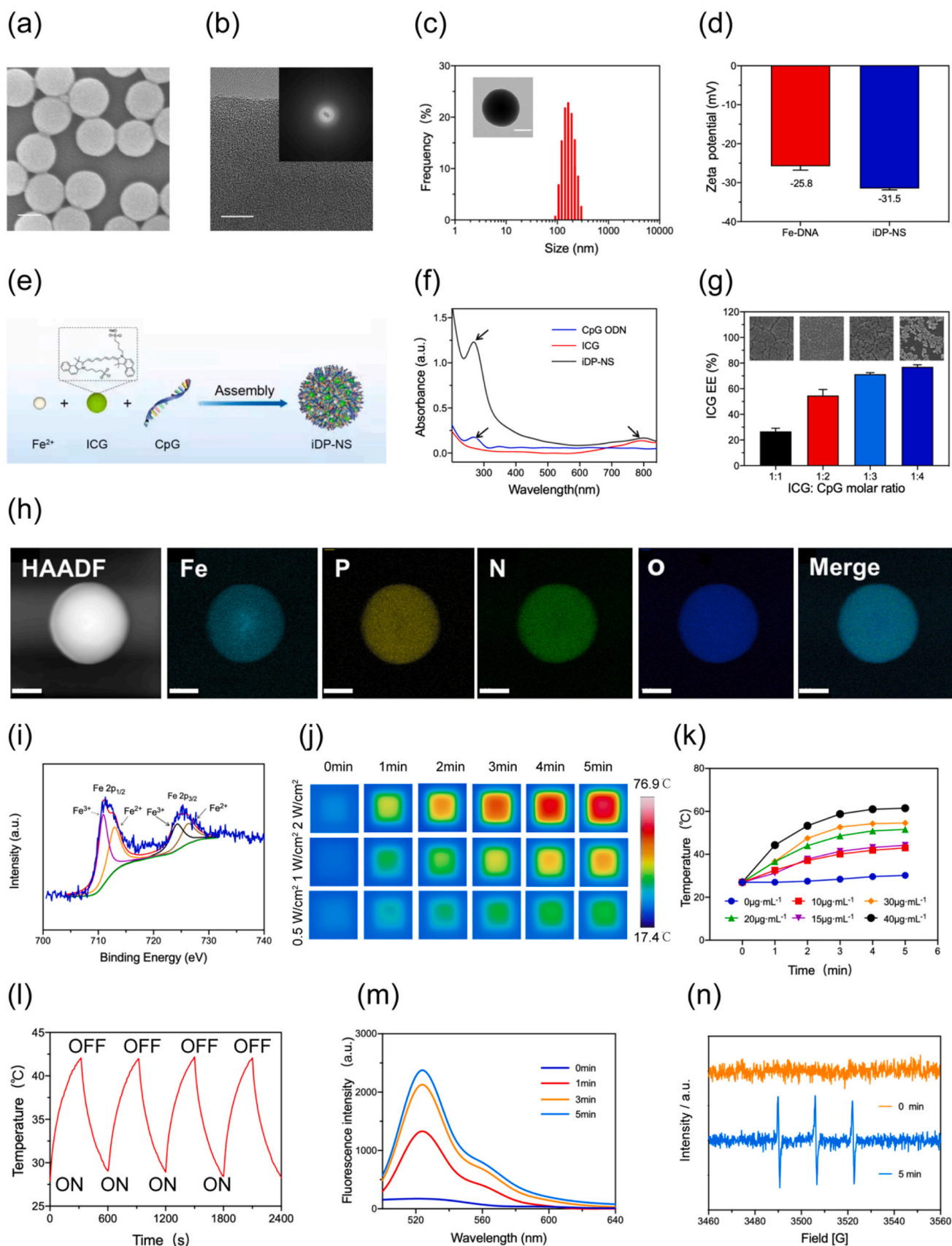
(caption on next page)

Fig. 1. Preparation and characterization of iDP-NS. (a) SEM image and (b) HRTEM image of iDP-NS. The inset in (b) shows FFT patterns of iDP-NS. (c) Number-averaged diameters of iDP-NS. The inset in (c) shows TEM image of iDP-NS , scale bar = 100 nm. (d) Zeta potential of Fe/DNA-NS and iDP-NS. (e) Schematic illustration of the preparation process for iDP-NS. (f) UV–vis absorption spectra of ICG, CpG ODN, and iDP-NS. (g) EE of ICG in the NPs with different added ratios of ICG: CpG in the synthesis. (h) HAADF-STEM image of iDP-NS, along with the corresponding EDS element maps for Fe, P, N, O and the overlay image of Fe, P, N, O. (i) Fe2p XPS spectrum of iDP-NS. (j) Infrared thermographs of iDP-NS aqueous solutions with different power density. (k) Temperature profile of iDP-NS with different ICG concentration. (l) Temperature profiles of iDP-NS aqueous solution for four ON/OFF cycles. (m) Evaluation of ROS generation at different irradiation times by iDP-NS using DCFH-DA as probes. (n) ESR spectra of the $^1O_2$ of iDP-NS without or with NIR light (808 nm, 2 W/cm^2) irradiation.
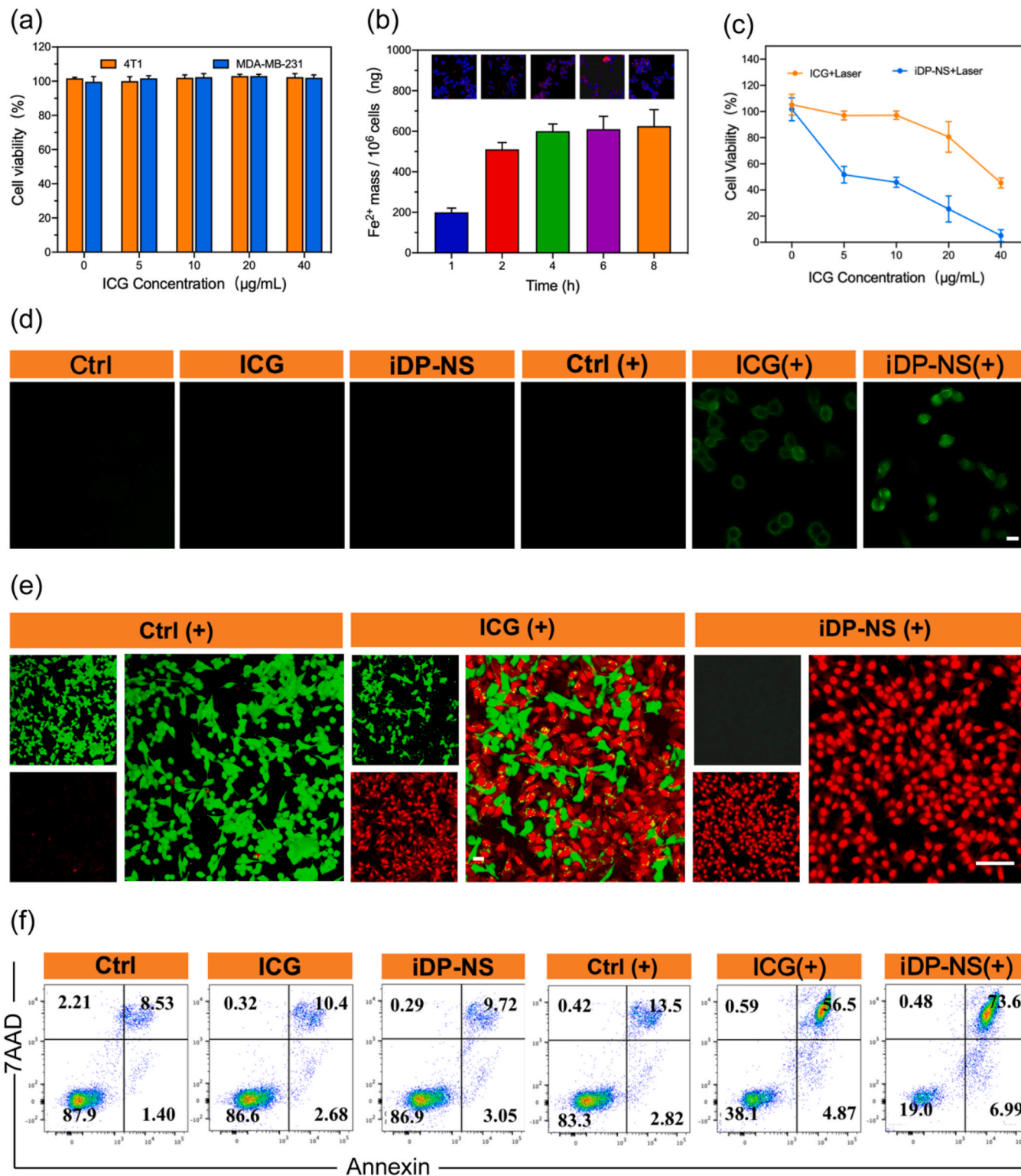

Fig. 2. *In vitro* photothermal/photodynamic antitumor performance of iDP-NS. (a) *In vitro* cell viability of 4T1 and MDA-MB-231 incubated with iDP-NS nanoparticles at various concentrations. (b) ICP-MS analysis and fluorescence images of 4T1 cells incubated with iDP-NS for multiple times. The cell images were performed immediately after the treatment. (c) Cell viability of 4T1 cells treated with ICG+Laser and iDP-NS+Laser at mutiple concentrations. (d) Intracellular ROS generation after different treatments. Scale bar: 40 µm. (e) Confocal laser scanning microscopy (CLSM) images of 4T1 cells stained by calcein-AM (green) and PI (red) after various treatments of Control, ICG+Laser, and iDP-NS +Laser. Scale bar: 100 µm. (f) Cell apoptosis analyzed by flow cytometry after mutiple treatments of Control, Control+Laser, ICG, ICG+Laser, iDP-NS and iDP-NS+Laser.
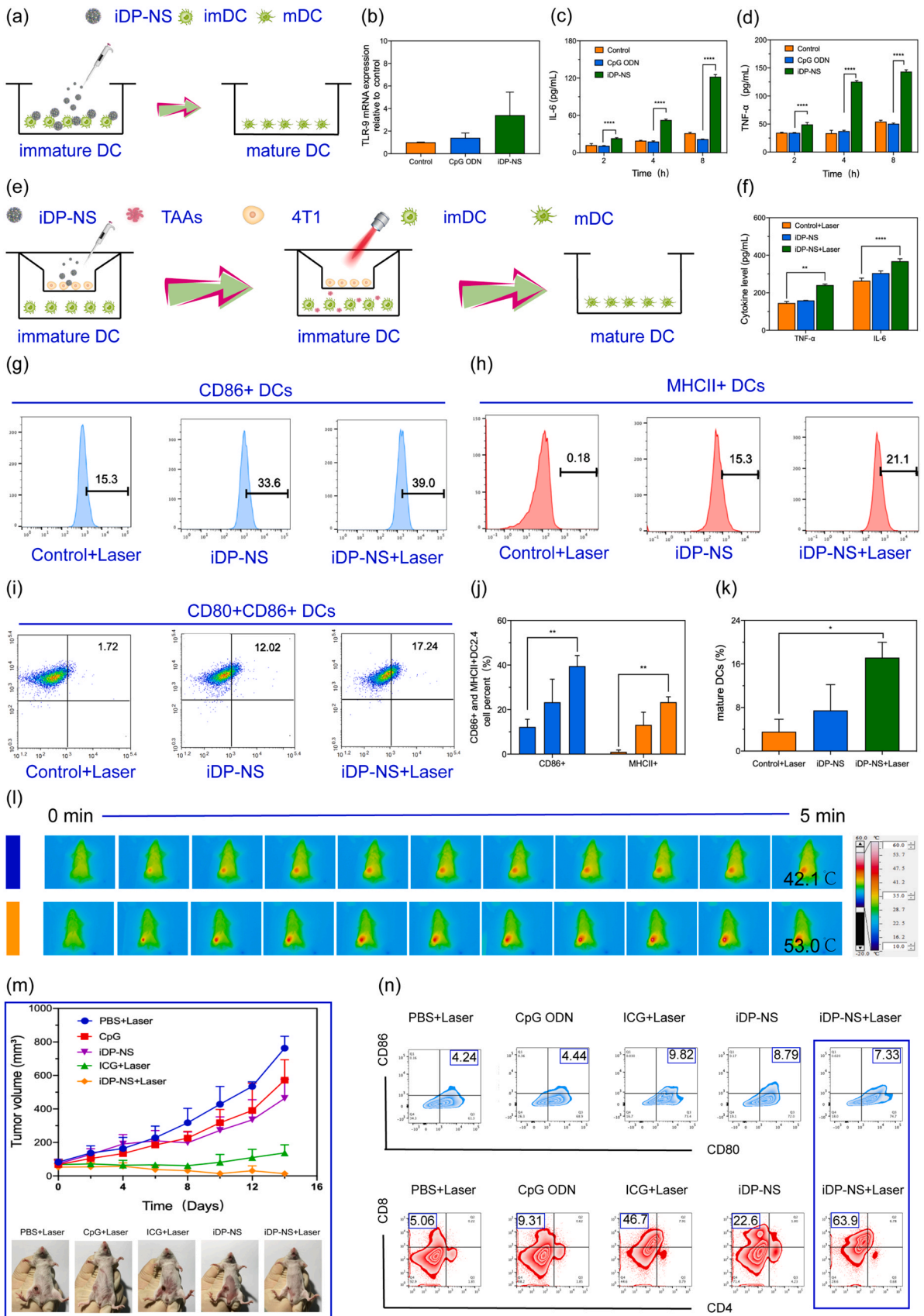
(caption on next page)

Fig. 3. Immune activation *in vitro* and *in vivo*. (a) Schematic illustration of DC2.4 coculture with iDP-NS. (b) RT-qPCR results showed the expression of TLR-9 in DC2.4 cells with different treatments. Cytokines of (c) IL-6 and (d) TNF-α in the DC 2.4 cells culture supernatant were measured by ELISA. (e) Schematic illustration of the transwell system-based evaluation process for DC2.4–4T1 tumor cells coculture, the vaccines were illuminated with 808 nm laser for 5 min at a power density of 2 W/cm². (f) Secretion of cytokines in the DC 2.4 cells culture supernatant of transwell system measured by ELISA. (g-h&j) Expression levels quantification of expression levels of MHCII and CD86 on the surface of DC2.4 after various treatments in transwell system. (i) iDP-NS induces DC maturation *in vitro*. (k) The frequency of mature DCs (CD11c+CD80 +CD86 +) *in vitro* upon different treatments. (l) IR thermal images of 4T1 residue tumor-bearing mice with 808 nm laser irradiation. (m) Average tumor growth curves of the tumors receiving various treatments (n = 5). (n) The frequency of mature DCs and CD8 +T cells in tumors upon different treatments. Data are mean ± SD; N = 5. ns: P > 0.05, *P < 0.05, **P < 0.01, ***P < 0.001. **** p < 0.0001.

successful ICG encapsulation (Fig. 1d). Furthermore, the characteristic absorption peaks of ICG at approximately 778 nm and CPG ODN at approximately 260 nm and the UV–vis absorption spectrum of iDP-NSs showed typical characteristic peaks of two molecules, which further suggested that the iDP-NS were successfully prepared (Fig. 1f). The high-angle annular dark-field scanning TEM energy-dispersive X-ray spectroscopy (HAADF-STEM-EDS) elemental mapping image and EDS line scanning of a single iDP-NS, in the presence of P, N, O and Fe, indicated that these nanospheres had been successfully prepared (Fig. 1h and S2). To further explore the regular synthesis of iDP-NS spheres, we coordinated the ratio of ICG to CpG ODN to synthesize nanospheres. Ingeniously, each collocation led to spherical-shaped nanoparticles that were well distributed. When the ICG: CpG ODN ratio was within a special range, the encapsulation efficiency (EE) of the ICG increased at the same time (Fig. 1 g). Since we intended to use phototherapy-immunotherapy with these iDP-NSs to prevent tumor recurrence and metastasis, the excellent photothermal effect was expected to ablate tumor tissue and induce immunotherapy. Considering these expectations, we investigated whether the photothermal conversion ability of ICG in the synthesized nanoparticles is affected by other components. In the high-resolution iron spectrum, Fe 2p3/2, the presence of the signal is assigned to Fe^{II} and Fe^{III} (Fig. 1i). After 2 W/cm² laser irradiation for 5 min, as shown in Figs. 1j and 1k, the photothermal effect of the iDP-NSs showed high concentration-dependent, time- dependent and power density-dependent. As shown in Fig. 1l, after four ON/OFF irradiation cycles at 2 W/cm², the iDP-NSs exhibited a high photothermal effect, and the NIR absorbing ability of the iDP-NSs did not change during this process. In addition, ICG with 808 nm laser irradiation can trigger the photodynamic response. Accordingly , we evaluated the ROS level of iDP-NSs. Herein , we used 2,7-dichloroflurescein probes (DCFHs) to detect the production of reactive oxygen species (ROS). As shown in Fig. 1m, the fluorescence intensity increased with the irradiation time prolonging, the fluorescence increasement. Moreover , hydroxyphenyl fluorescein (HPF) probes were applied to detect the production of·OH. We found the iDP-NSs with 808 nm laser irradiation do not trigger the production of·OH (Fig. S4). Next, electron spin resonance (ESR) assay was employed to analyze $^1O_2$. After iDP-NSs were irradiated for 5 min, we found strong and evident ESR characteristic peaks of $^1O_2$ (Fig. 1 n). Overall , the powerful photodynamic and photothermal performance of iDP-NSs has the potential to combat breast cancer. As shown in Fig. S5, the SEM images illustrated that iDP-NSs remained nanosphere structure for 4 h. With prolonged time, the nanosphere in PBS and FBS gradually changed. We found that the drug has a faster and higher release rate in acidic environments, and this feature will help iDP-NS get a certain controlled release effect and improve the bioavailability of drugs in the tumor microenvironment (Fig. S6).
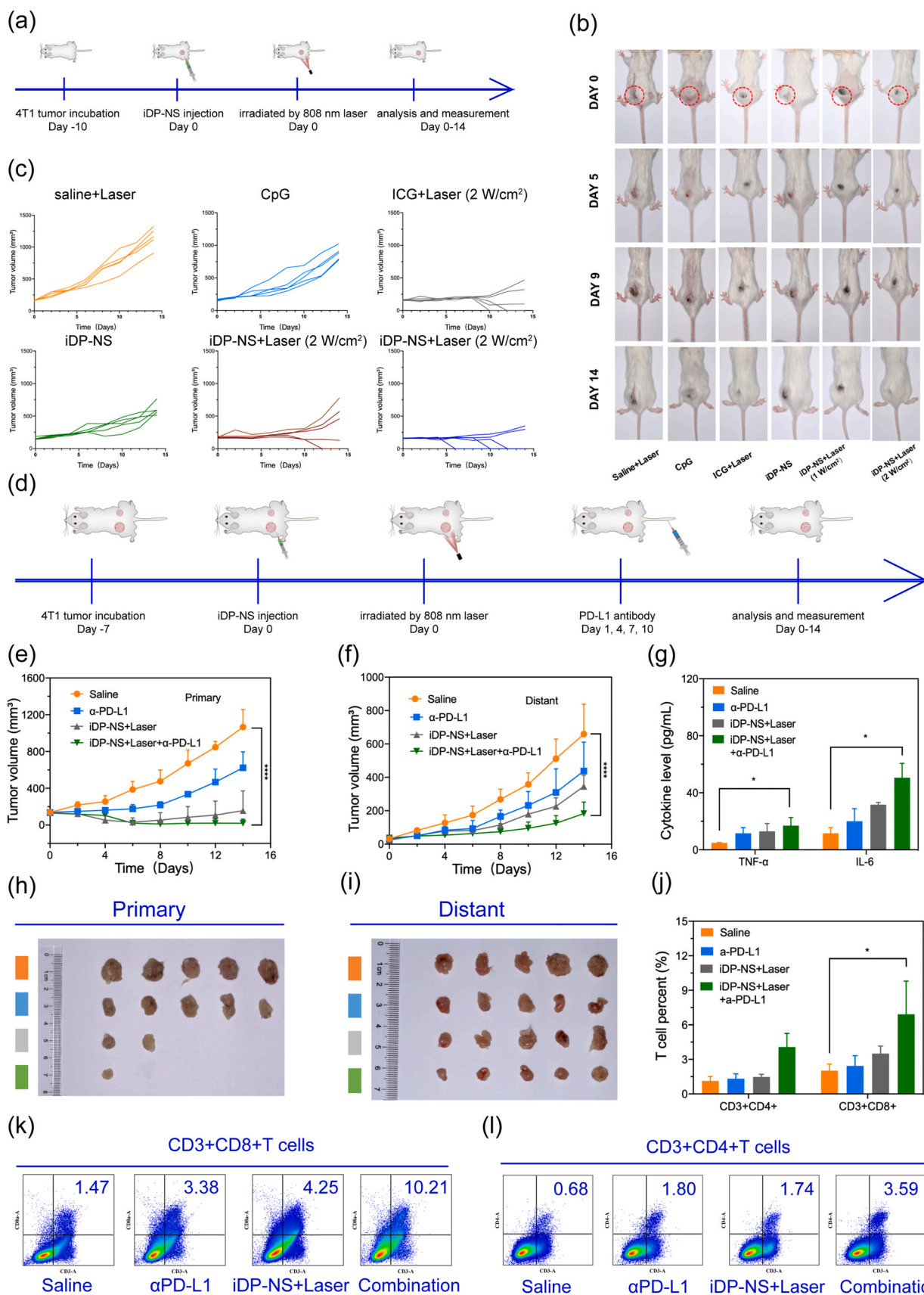
In vitro photothermal/photodynamic antitumor performance of iDP-NS

Although the three components that make up iDP-NSs have been previously proven to have good biocompatibility previously, it was still necessary to evaluate the biosafety of the synthetic materials [19,25,26]. Therefore, we chose two types of breast tumor cells and immune cells to evaluate the cytotoxicity of iDP-NSs by Cell Counting Kit-8 (CCK-8) assay. MDA-MB-231、4T1、RAW264.7 and

DC2.4 cells were incubated with different concentrations of iDP-NSs for 24 h. As shown in Fig. 2a and S7, the material induced low cytotoxicity within a specific concentration range, and the cell survival rate was as high as 95%. Inductively coupled plasma mass spectrometry (ICP-MS) analysis and confocal laser scanning microscopy (CLSM) images confirmed that the cellar iDP-NSs have a significant increase within 4 h and a slight change after 4 h (Fig. 2b). Accordingly, we determined the viability of 4T1 treated with ICG and iDP-NS after irradiation. The results indicated that iDP-NS+Laser showed a more apparent cytotoxic effect than ICG+Laser at the same ICG concentration (Fig. 2c). Based on this, reactive oxygen species (ROS) induced by the ICG component in iDP-NSs in response to near-infrared light irradiation led to cell death. DCFH-DA can be used as a fluorescent probe of reactive oxygen species to verify the total reactive oxygen species production in living cells directly. The DCFH-DA probe was used to detect the ROS production in the cells in different treatment groups. The results showed that the green fluorescence signal of iDP-NS+Laser group was much higher than other groups. This conclusion indicated that the iDP-NS+Laser group generated a certain level of reactive oxygen species in the cytoplasm, while the fluorescence signal detected in the ICG+Laser group was much weaker than that in the iDP-NS+Laser group (Fig. 2d). Furthermore, we used CLSM to observe the ratio of dead and live cells after different treatments. We used the calcein acetoxymethyl ester (calcein-AM) and propidium iodide (PI) live-dead staining method to verify the death rate of 4T1 tumor cells induced by the iDP-NS+Laser. Red and green represent dead cells and live cells, respectively. Fig. 2e shows that the iDP-NS+Laser exhibited a more significant killing effect on tumor cells than the other treatments. In addition, we further analyzed the phototoxicity of each group by Annexin-7AAD flow cytometry, and the percentages of apoptotic and necrotic in the iDP-NS-irradiated group were significantly higher than those in the other groups (Fig. 2f). These results indirectly indicate that iDP-NS have an efficient photosensitizer delivery capability. Overall, these results lay the foundation for the iDP-NS nano-vaccine to kill tumors and regulate the immune response in the tumor microenvironment.

Immune activation in vitro and in vivo

DCs are the most important antigen-presenting cells and play an important role in antitumor immunity [11,19–21]. Elevating the DC cell maturation rate is a direct method for determining the relationship between iDP-NSs and the immune system *in vitro*. First, we incubated DCs with various materials to compare the internalization of free CpG ODNs relative to iDP-NSs (Fig. 3a). Fig. 3b showed that the expression level of TLR-9 mRNA in the iDP-NS group was higher. The experimental results showed that free CPG ODNs exerted almost no activating effect on TLR-9 receptors. This outcome resulted from free nucleic acid negatively charges, inhibiting their easy penetration of cell membranes. Furthermore, TLR-9 was more easily activated, and the expression level of TLR-9 mRNA was higher. Mature DCs secrete immune-related cytokines, and we used an ELISA kit to detect the concentration of cytokines in the culture supernatant. After iDP-NS treatment, the levels of secreted TNF-α and IL-6 were largely enhanced comparing with that in the free DNA group, which was consistent with the RT–PCR results (Figs. 3c-3d). These results showed that the concentration of cytokines gradually increased at different times, proving that synthetic iDP-NSs

(a)

(b)

(c) saline+Laser   CpG   ICG+Laser (2 W/cm²)

iDP-NS   iDP-NS+Laser (2 W/cm²)   iDP-NS+Laser (2 W/cm²)

(d)

(e) (f) (g)

(h) Primary   (i) Distant   (j)

(k) CD3+CD8+T cells   (l) CD3+CD4+T cells

(caption on next page)

Fig. 4. Antitumor immune response *in vivo*. (a) Schematic illustration of *in vivo* photo-immunotherapy. (b) Typical photographs of mice to evaluate the antitumor effect of 4T1 tumor after various treatments (n = 5). (c) Individual tumor growth curves of the tumors receiving various treatments (n = 5). (d) Schematic illustration of the anti-tumor immune response of iDP-NS-mediated phototherapy immune effect combined with α-PD-L1. (e&h) Growth curves of (e) primary tumors and primary photographs (h) in 4T1 tumor-bearing mice after different treatments. (f&i) Growth curves of (f) distant tumors and Photographs (i) in 4T1 tumor-bearing mice after different treatments. (g) TNF-α and IL-6 levels were detected by ELISA assay in the serum of mice after different treatments. (k&l) The percentage of tumor-infiltrating CD4 + T cells and CD8 + T cells in distant tumor cells. (j) Quantitation of CD8 + T cells and CD4 +T cells in the distant tumor. (1) Saline, (2) α-PD-L1, (3) iDP-NS+Laser, (4) iDP-NS+Laser+ α-PD-L1. Data are mean ± SD; N = 5. ns: P > 0.05, *P < 0.05, **P < 0.01, ***P < 0.001. ****p < 0.0001.

effectively promoted the maturation of DC cells, which are the most important antigen-presenting cells and play important roles in antitumor immunity. Immature DCs capture antigens in the surrounding fluid and convert them into peptides during migration to nearby draining lymph nodes, where they present the major histocompatibility complex (MHC) with the peptides to the T cell receptor (TCR) to activate T cells [27,28]. Examining the DC maturation rate is a direct method of evaluating the relation between iDP-NSs and the immune system in vitro. subsequently, we used a transwell system to detect the maturation of DCs. The design of our i*n vivo* experiment is shown in Fig. 3e. The typical markers of mature DCs are CD86 and MHCII, and they were examined by flow cytometry (Figs. 3g-3h&3j). After the transwell system cells were treated with various materials, but only the iDP-NSs induced moderate DC maturation (Fig. 3i and k). In contrast, iDP-NS+Laser significantly promoted DC maturation in the system, the results attribute to the release of tumor-associated antigens after iDP-NS with irradiation. Moreover, cytokines can indirectly reflect the DC maturation-induced systemic immune response, which was further evaluated by measuring the concentration of cytokines by enzyme-linked immunosorbent assays (ELISAs). Notably, tumor necrosis factor-α (TNF-α) and interleukin-6 (IL−6) were obviously higher in the iDP-NS+L group than in the iDP-NS group (Fig. 3f). These results showed that dual phototherapy led to the release of tumor-associated antigens (TAAs), and combined with CpG ODNs, induced a particularly powerful immune response.

To further investigate whether iDP-NS vaccines can facilitate DCs maturation *in vivo* , the orthotopic 4T1 tumor models were established to assess the antitumor immune response. The tumor-bearing mice were divided into 5 groups: PBS+Laser, CpG ODN, ICG+Laser, iDP-NS and iDP-NS +Laser. When the tumor grew to about 100 mm^3, different samples were injected into the tumor site by intratumoral injection, with the dose of ICG and CpG ODN is 1 mg/kg and 5 mg/kg, respectively. After 4 h, the injection sites were irradiated with 808 nm laser for 5 min at a power density of 2 W/cm^2 (Fig. 3l). Temperature of iDP-NS+Laser reached 53 °C. Changes in tumor volume were measured every other day during treatment. After treatment, the maturation rate of DC and T cell infiltration of tumor tissues were measured. As shown in Fig. 3m-n, iDP-NS +Laser eradicated tumors and promoted the maturation of DC cells and the infiltration of T cells compared with other groups. It is worthy that iDP-NS showed a stronger anti-tumor immune response than free CpG ODN. iDP-NS combined with laser showed the strongest immune activity. The results were consistent with those of *in vivo* experiments.
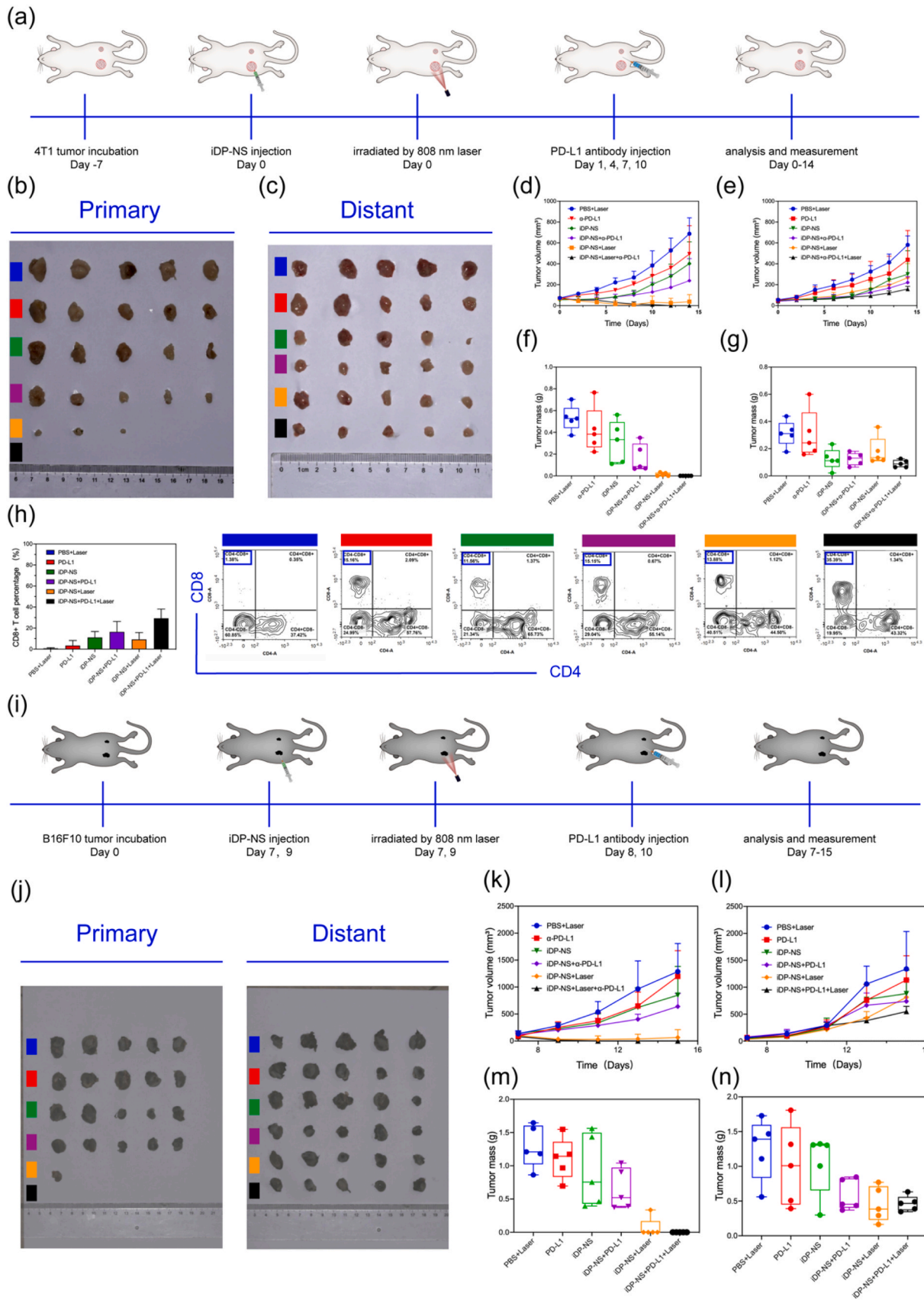
Antitumor immune response in vivo

Though *in vitro* experiments, considering the good biocompatibility and strong immune response of iDP-NSs, we were encouraged to further explore their potential anticancer value *in vivo*. We hope that this iDP-NSs nano "vaccine" can effectively kill tumors and prevent local tumor recurrence. Through subcutaneous inoculation, 1×10^6 4T1 cells were injected into the left back of BALB/c mice to establish a single 4T1 breast tumor model (Fig. 4a). When the tumor volume reached 100–200 mm^3, saline, free CpG ODNs, free ICG, and iDP-NSs were injected into the tumor *in situ*. Then, the light therapy group was subjected to light therapy with a power density of 2 W/cm^2 radiation for 5 min. First, the PTT treatment effect of iDP-NSs on tumor-bearing mice was evaluated by monitoring the temperature

of the tumor sites. For the iDP-NS NIR laser irradiation group, the temperature of the injection site rose to approximately 60 °C under 808 nm laser irradiation, which had the potential to kill the tumor cells *in situ* (Fig. 4b and S8). This result also showed that the excellent photothermal effect of this nano "vaccine" can be applied to tumor treatment *in vivo*. In addition, a picture of the tumor site in mice was taken to assess the growth and development of the tumor (Fig. 4c). For two weeks, the tumor volume and weight changes in the mice were monitored every two days. The results confirmed that the iDP-NS group conferred greater protection against tumor growth (Figs. 4d-4e). This outcome may have been a result of iDP-NSs effectively improving antigen presentation in the tumor microenvironment and triggering a strong immune response, promoting the infiltration of T cells and significantly inhibiting tumor growth. The body weight changes in the mice were shown in Fig. S9. The mouse receiving treatment has no obvious body weight changes, indicating that the drug has good biocompatibility. In addition, histopathological examination and morphological analysis of all major organs and tumor tissues were performed during treatment. As shown in Fig. S10, there was no pathological change in the important organs of the mice, which further showed the histocompatibility of the material.

To determine whether iDP-NSs can trigger antitumor immunity to make tumors more sensitive to ICB, we used iDP-NSs combined with anti-PD-L1 antibodies to combat 4T1 tumors. The primary tumors were injected with iDP-NSs with or without 808 nm laser irradiation, while the remote tumors were not directly treated. After irradiation, the mice were treated with α-PD-L1 blocking on the first, fourth, 7th and 10th days (Fig. 4d). The antitumor effect was evaluated by the growth rate of the primary tumor and distant tumors. As shown in Fig. 4e & h, the growth of the primary tumors in the iDP-NS+Laser and iDP-NS+Laser groups was completely suppressed. At the same time, the iDP-NS+Laser group also effectively inhibited growth of distant tumors (Fig. 4f & i). These results further showed that the iDP-NSs plus α-PD-L1 group not only exhibited effective inhibitory ability on local tumors but also effectively inhibited the proliferation of distant tumors compared to the groups that received iDP-NS+Laser or α-PD-L1 only (Fig. S11). None of the treated mice showed obvious body weight changes, indicating that the drug had good biocompatibility (Fig. S12). These results showed that iDP-NS-mediated tumor-specific immunity responded to PD-L1-blocking immunotherapy and the immunotherapy strategies combined with iDP-NSs and PD-L1 antibody may offer prospect for patients undergoing metastatic breast cancer.

To further clarify the underlying immunological mechanisms, we used flow cytometry to study the systemic antitumor immunity of 4T1-bearing mice receiving different treatments. The results showed that the percentages of CD8 + T cells and CD4 + T cells in distant tumors of the mice receiving iDP-NS+Laser+ α-PD-L1 were significantly increased compared to other groups (Fig. 4j-l&S13). Furthermore, the serum levels of IL-6 and TNF-α also showed significant upregulation in mice after iDP-NS+Laser+ α-PD-L1 treatment (Fig. 4g). The combination of iDP-NS-mediated antigen presentation and α-PD-L1 effectively generated a systemic immune response through immune activation and T cell infiltration. These results indicated that iDP-NSs potentially induced antitumor humoral immune responses and that PD-L1 checkpoint blockade plays an important role in promoting T cell infiltration and controlling distant tumors. In conclusion, we demonstrated that iDP-NS-mediated dual phototherapy and CpG

(caption on next page)

Fig. 5. Abscopal effect of iDP-NS combined with ICB. (a) Schematic illustration of the anti-tumor immune response of iDP-NS-mediated phototherapy immune effect combined with α-PD-L1 in BALB/c abdominal tumor-bearing 4T1 model. (b-c) Bilateral tumors images in BALB/c abdominal tumor-bearing 4T1 model after different treatment. (d-e) Growth curves of bilateral tumors in BALB/c abdominal tumor-bearing 4T1 model after different treatment. (f-g) Tumor masses of bilateral tumors in BALB/c abdominal tumor-bearing 4T1 model after different treatment. (h) The percentage of tumor-infiltrating CD4 + T cells and CD8 + T cells in distant tumor cells. (i) Schematic illustration of the anti-tumor immune response of iDP-NS-mediated phototherapy immune effect combined with α-PD-L1 in C57BL/6 abdominal tumor-bearing B16F10 model. (j) Bilateral tumors images in C57BL/6 abdominal tumor-bearing B16F10 model after different treatment. (k-l) Growth curves of bilateral tumors in C57BL/6 abdominal tumor-bearing B16F10 model after different treatment. (m-n) Tumor masses of bilateral tumors in C57BL/6 abdominal tumor-bearing B16F10 model after different treatment. Data are mean ± SD; N = 5. ns: P > 0.05, *P < 0.05, **P < 0.01, ***P < 0.001. **** p < 0.0001.

delivery can enhance antigen presentation. iDP-NS-mediated dual phototherapy induced ICD, releasing tumor debris, including TAAs, and CpG ODNs promote the maturation of DCs. The efficient antigen presentation ability of the iDP-NSs in the tumor microenvironment and immune checkpoint blockade therapy synergistically produced systemic and persistent immune effects.

Abscopal effect of iDP-NS combined with ICB

To further verify iDP-NSs with 808 nm laser irradiation combined with ICB could enhance systemic antitumor immunity, we evaluated the abscopal effect of iDP-NS in combination with ICB in two mouse models. First, we evaluated whether our nano "vaccine" with the ICB therapy could induce systemic immune response in bilateral BABL/c abdominal-tumor-bearing 4T1 model. Then, we assess the abscopal effect in the group treated with PBS+Laser, α-PD-L1, iDP-NS, iDP-NS + α-PD-L1, iDP-NS+Laser, iDP-NS+Laser+α-PD-L1. The left tumors (primary) were treated with mutiple properties, while the right (distant) tumors were untreated (Fig. 5a). The mice then received α-PD-L1 immune checkpoint blockade therapy. As shown in Figs. 5b-5g, iDP-NS+Laser synergized with α-PD-L1 could effectively control the growth of primary tumors and untreated distant tumors, indicating iDP-NS with 808 laser irradiation can elicit powerful immune response. Then, we investigated the T cells infiltration in distant tumors , in order to determine the immune activation efficiency of iDP-NS+Laser+ α-PD-L1. As shown in Fig. 5h, iDP-NS+Laser + α-PD-L1 triggered the most powerful T cells infiltration.

We then studied the abscopal effect triggered by the combination of iDP-NS+Laser and α-PD-L1 on bilateral B16F10 tumor-bearing C57BL/6 model. On day 0, the 6-week-old female mice were inoculated subcutaneously with B16F10 cells on their abdomen. On day 7, the abdominal B16F10 tumor-bearing C57BL/6 mice were randomly divided six groups: PBS+Laser, α-PD-L1, iDP-NS, iDP-NS+ α-PD-L1, iDP-NS+Laser, iDP-NS+Laser+α-PD-L1. On day 7,9, the mice received intratumoral injection of materials and irradiated with 808 nm laser. Subsequently, the mice received intraperitoneal injection of α-PD-L1. The primary tumors were administrated with iDP-NS with or without 808 nm laser irradiation, while the other tumor remained untreated (Fig. 5i). The abscopal effect of iDP-NS with 808 nm laser combined with ICB was evaluated depending on the growth rates of bilateral tumors. As shown in Fig. 5j-n , the iDP-NS+Laser+ α-PD-L1 group not only effectively killed the primary tumors , but also inhibited the proliferation of distant tumors.

Long-term immune response

The iDP-NS-mediated photodynamic-immune response combined with ICB not only obliterated the primary tumor but also suppressed the distant tumors. We further explore the immune memory effect of iDP-NS, we want to know whether the regime of iDP-NS+Laser combined with ICB could inhibit the tumor recurrence, lung metastasis and rechallenge after surgical therapy (Fig. 6a). As shown in Fig. 6b, the lung tissue images showed that the mice in the PBS+Laser group had different numbers of metastatic nodules, while the lung tissues in the iDP-NS+Laser+ α-PD-L1 group were relatively healthy. As shown in Fig. 6c, the H&E staining results of lung tissues further proved the above results. Fig. 6d-e showed that the lung mass and the number of nodules of the mice in the iDP-NS+Laser+ α-

PD-L1 group compared with the untreated group were reduced. As shown in Fig. 6g-h, the recurrence of the primary tumor can be seen in the mice treated with PBS+Laser, while only one can be seen in the mice treated with iDP-NS+Laser+ α-PD-L1. As shown in Fig. 6i, iDP-NS+Laser+ α-PD-L1 was more effective in inhibiting secondary distal tumors than the control treatment. Lung metastasis is another thorny problem faced by breast cancer surgery patients. Observing the lung metastasis of patients undergoing surgery is an important factor to evaluate the treatment effect. As shown in Fig. 6f, within 35 days, all mice in the PBS+Laser group died, while only one mouse in the iDP-NS+Laser+ α-PD-L1 group died. The above results suggest that the photodynamic-immune response mediated by iDP-NS can not only clear the primary tumor but also induce a strong immune memory.

The photodynamic-immune response mediated by iDP-NS after irradiation combined with ICB therapy provides long-term and effective immune protection for breast cancer patients after surgery. Intratumoral injection therapy can ensure a greater accumulation of nanoparticles at the tumor site to kill cancer cells and generate a strong immune response. Photodynamic therapy combined with immunotherapy and surgery therapy effectively removes primary tumors and inhibits the recurrence and lung metastasis of primary tumors and secondary tumor growth. In conclusion, this therapeutic strategy can provide a new reference for the use of nano "vaccine" to treat postoperative breast cancer patients and enhance immune memory.

Notably, iDP-NS is a photosensitive immune vaccine that requires strict light avoidance during injection. iDP-NSs combined with an anti-PD-L1 antibody can effectively suppress the relapse of local breast cancer and inhibit the development of metastatic tumors through synergistic photothermal/photodynamic therapy and immunotherapy [29–33]. First, this new vaccine can effectively eliminate local tumors in a short period with *in situ* injections and remove remaining tumors with immunotherapy. Second, PDT/PPT itself can initiate an immune response by inducing the maturation of DCs and the infiltration of T cells. Third, in contrast to free CpG ODNs, the iDP-NS immune vaccine significantly improves the stability of CpG ODNs *in vivo* and DC absorption efficiency, subsequently activating DCs.

Immunogenic cell death involves the transformation of tumor cells into immunogenic cells [34–36]. In addition, tumor cells undergo apoptosis and stimulate antitumor immune effects in the body. In contrast to other cell death modalities, the release of endogenous danger signals and tumor-associated antigens promote the activation of dendritic cells and the infiltration of toxic T cells, promoting tumor elimination [37]. Photodynamic therapy can cause immunogenic necrosis of tumor cells [38–40]. Preclinical research and clinical studies have confirmed that photodynamic therapy generates cancer adaptive immune response through the immunogenic cell death pathway. The tumor-specific T-cell response is induced to further enhance the immune response by facilitating the maturation of dendritic cells. Therefore, the iDP-NS immune vaccine can be considered an autologous cancer vaccine *in situ*, using the entire tumor cell as a source of tumor antigens. Once damaged tumor cells are secreted, they led to increased production of adaptive antitumor immune antigen-presenting cells and cytokines by promoting DC maturation [41,42]. The immunotherapeutic effect of photothermal ablation during tumors is worth further exploration.
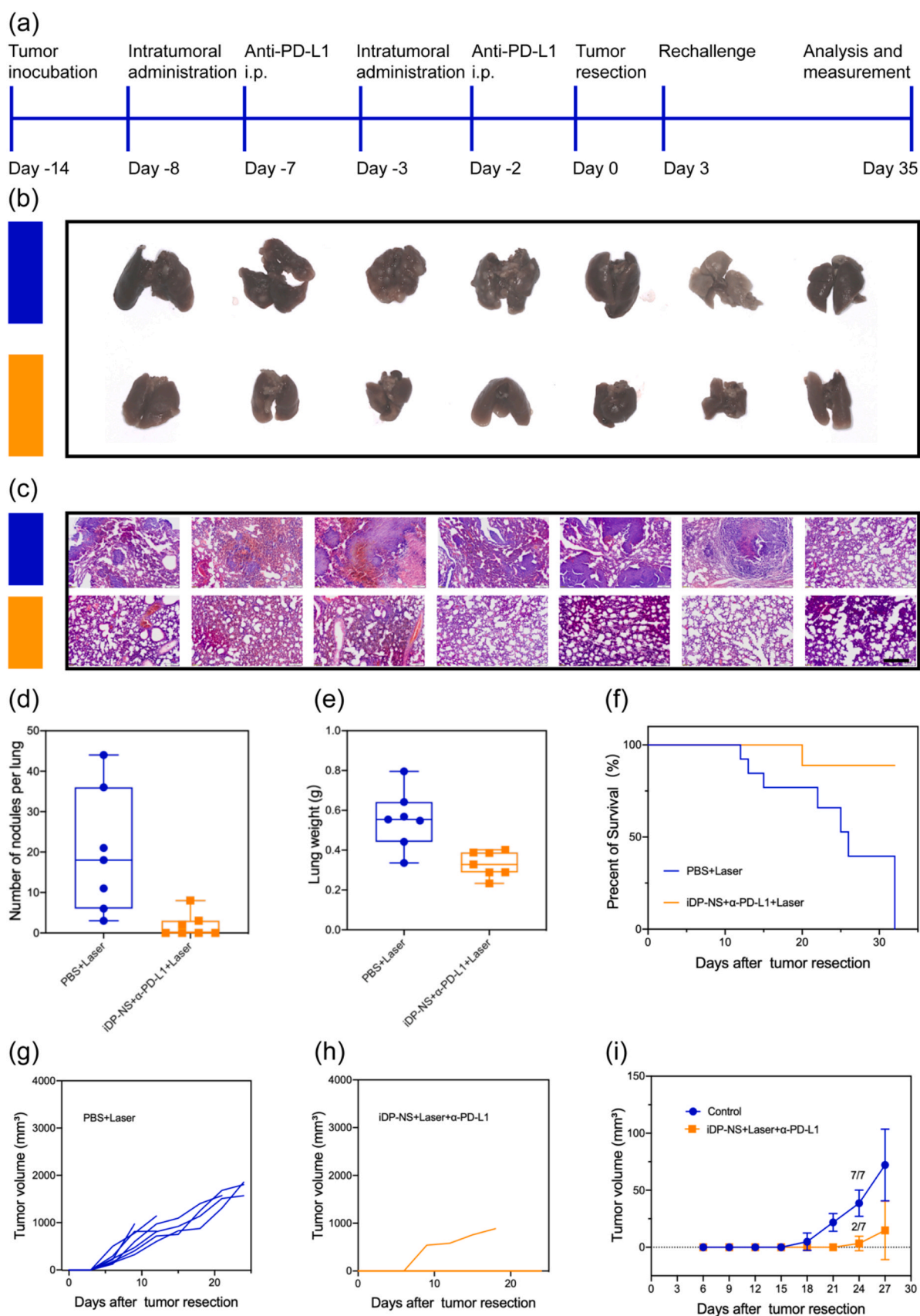
Fig. 6. Long-term immune response. (a) Schematic illustration of the 4T1 tumor recurrence, lung metastasis and rechallenge studies. (b) Photographs of 4T1 lung metastatic nodules for mice after various treatments (n = 7). (c) H&E staining image of 4T1 lung issues for mice after various treatments (n = 7). (d) Lung metastatic nodules on the lung surface (n = 7). (e) Weight of lung issues (n = 7). (f) Survival curve of PBS+Laser and iDP-NS+Laser+ α-PD-L1 (n = 7). (g-h) Growth curves for recurrent tumors in mice receiving different treatments. (i) Growth curves for secondary tumors in mice receiving different treatments.

Conclusion

Postoperative tumor recurrence and distant metastasis are fatal to breast cancer patients. In recent years, immunotherapy has emerged as a promising strategy for protecting patients against tumor relapse and metastasis. In this study, we demonstrated that iDP-NSs combined with immune checkpoint blockade therapy has unique advantages over other immunotherapy regimens. First, rationally developed iDP-NSs initiate antigen release and a tumor-specific immune response through NIR-triggered cancer immunotherapy. At the same time, iDP-NSs loaded with CpG immune adjuvants activate TLR9 receptors. This nano vaccine is simple to prepare, cost-effective, and easy to store. Second, this nano vaccine combined with PD-L1 antibody not only can effectively inhibit the recurrence and metastasis of *in situ* tumors but can also exert a powerful inhibitory effect on the growth of distant tumors. These tumor treatments may be more effective than commonly used tumor therapies because they kill *in situ* tumors while stimulating patients to produce effective and long-lasting anticancer responses. Third, in recent years, the effects of tumor immunotherapy have been severely limited in the tumor microenvironment. iDP-NSs combined with immune checkpoint blockade (ICB) therapy can effectively overcome tumor cell escape. In addition, NIR lasers can be used to irradiate cells deep within tumors, addressing other shortcomings caused by the failure of other light forms to fully penetrate deep tumors. Hence, this new nano-vaccine is expected to undergo clinical transformation.

In summary, we developed a photosensitizer and nucleic co-delivery therapeutic platform using a simple biomimetic approach. The nanoparticle synthesis method is a one-pot reaction of FeII ions, CpG and ICG, which is extremely simple. Thus, it has excellent application prospects. Most of all, iDP-NS has ultrahigh loading content, uptake rate and a highly tunable ratio, leading to a remarkable curative effect. The intertwining DNA photosensitizer vaccine exhibited an ultrahigh loading rate and excellent delivery efficiency with the two molecules used. Mostly , ICG mediated phototherapy triggers immunogenic cell death to release TAAs with activation of the TLR9 pathway commonly promoting DCs maturation. Moreover, NIR laser-triggered iDP-NSs vaccine synergizes with CBI elicited a sustained produce systemic immune effect, which effectively suppressed tumor recurrence and metastasis after vaccination , the advanced nano "cancer vaccine" is extremely promising for use in developing a multifunctional cancer vaccine delivery system.

CRediT authorship contribution statement

Guohui Yu: Conceptualization, Methodology, Investigation, Data curation, Formal analysis, Writing – review & editing. **Fan Dong:** Conceptualization, Methodology, Investigation, Data curation, Formal analysis, Writing – review & editing. **Wenshu Gong:** Conceptualization, Methodology, Investigation, Data curation, Formal analysis, Writing – review & editing. **Lisha Sun:** Conceptualization, Methodology, Investigation. **Ning Du:** Conceptualization, Methodology, Investigation. **Ningyu Li:** Conceptualization, Methodology, Investigation. **Hao Dai:** Conceptualization, Methodology, Investigation. Lei Shi: Supervision, Writing – review & editing. **Yuguang Wang:** Supervision, Writing – review & editing.

Declaration of Competing Interest

The authors declare that they have no known competing financial interests or personal relationships that could have appeared to influence the work reported in this paper.

Appendix A. Supporting information

Supplementary data associated with this article can be found in the online version at doi:10.1016/j.nantod.2022.101498.

References

[1] M. Vanneman, G. Dranoff, Combining immunotherapy and targeted therapies in cancer treatment, Nat. Rev. Cancer 12 (2012) 237–251.

[2] D.S. Chen, I. Mellman, Oncology meets immunology: the cancer-immunity cycle, Immunity 39 (2013) 1–10.

[3] X. Duan, C. Chan, W. Han, N. Guo, R.R. Weichselbaum, W. Lin, Immunostimulatory nanomedicines synergize with checkpoint blockade immunotherapy to eradicate colorectal tumors, Nat. Commun. 10 (2019) 1899.

[4] X. Sun, Y. Zhang, J. Li, K.S. Park, K. Han, X. Zhou, Y. Xu, J. Nam, J. Xu, X. Shi, L. Wei, Y.L. Lei, J.J. Moon, Nat. Nanotechnol. 16 (2021) 1260–1270.

[5] N. Ioannou, P.R. Hagner, M. Stokes, A.K. Gandhi, B. Apollonio, M. Fanous, D. Papazoglou, L.A. Sutton, R. Rosenquist, R.M. Amini, H. Chiu, A. Lopez-Girona, P. Janardhanan, F.T. Awan, J. Jones, N.E. Kay, T.D. Shanafelt, M.S. Tallman, K. Stamatopoulos, P.E.M. Patten, A. Vardi, A.G. Ramsay, Blood 137 (2021) 216–231.

[6] S. Suresh, B. Chen, J. Zhu, R.J. Golden, C. Lu, B.M. Evers, N. Novaresi, B. Smith, X. Zhan, V. Schmid, S. Jun, C.M. Karacz, M. Peyton, L. Zhong, Z. Wen, A.A. Sathe, C. Xing, C. Behrens, Wistuba, G. Xiao, Y. Xie, Y.X. Fu, J.D. Minna, J.T. Mendell, K.A. O'Donnell, eIF5B drives integrated stress response-dependent translation of PD-L1 in lung cancer, Nat. Cancer 1 (2020) 533–545.

[7] R.S. Herbst, G. Giaccone, F. de Marinis, N. Reinmuth, A. Vergnenegre, C.H. Barrios, M. Morise, E. Felip, Z. Andric, S. Geater, M. Ozguroglu, W. Zou, A. Sandler, I. Enquist, K. Komatsubara, Y. Deng, H. Kuriki, X. Wen, M. McCleland, S. Mocci, J. Jassem, D.R. Spigel, Atezolizumab for First-Line Treatment of PD-L1-Selected Patients with NSCLC, N. Engl. J. Med 383 (2020) 1328–1339.

[8] J. Galon, D. Bruni, Approaches to treat immune hot, altered and cold tumours with combination immunotherapies, Nat. Rev. Drug Disco 18 (2019) 197–218.

[9] K. Lu, C. He, N. Guo, C. Chan, K. Ni, G. Lan, H. Tang, C. Pelizzari, Y.X. Fu, M.T. Spiotto, R.R. Weichselbaum, Low-dose X-ray radiotherapy-radiodynamic therapy via nanoscale metal-organic frameworks enhances checkpoint blockade immunotherapy W. Lin, Nat. Biomed. Eng. 2 (2018) 600–610.

[10] L. Cicchelero, H. de Rooster, N.N. Sanders, Various ways to improve whole cancer cell vaccines, Expert Rev. Vaccin. 13 (2014) 721–735.

[11] T. Wang, D. Wang, H. Yu, B. Feng, F. Zhou, H. Zhang, L. Zhou, S. Jiao, Y. Li, A cancer vaccine-mediated postoperative immunotherapy for recurrent and metastatic tumors, Nat. Commun. 9 (2018) 1532.

[12] H. Wang, X. Pan, X. Wang, W. Wang, Z. Huang, K. Gu, S. Liu, F. Zhang, H. Shen, Q. Yuan, J. Ma, W. Yuan, H. Liu, Degradable carbon-silica nanocomposite with immunoadjuvant property for dual-modality photothermal/photodynamic therapy, ACS Nano 14 (2020) 2847–2859.

[13] Y. Shao, B. Liu, Z. Di, G. Zhang, L.D. Sun, L. Li, C.H. Yan, Engineering of upconverted metal-organic frameworks for near- , infrared light-triggered combinational photodynamic/chemo-/immunotherapy against hypoxic tumors, J. Am. Chem. Soc. 142 (2020) 3939–3946.

[14] X. Duan, C. Chan, N. Guo, W. Han, R.R. Weichselbaum, W. Lin, Photodynamic therapy mediated by nontoxic core-shell nanoparticles synergizes with immune checkpoint blockade to elicit antitumor immunity and antimetastatic effect on breast cancer, J. Am. Chem. Soc. 138 (2016) 16686–16695.

[15] K. Lu, C. He, N. Guo, C. Chan, K. Ni, R.R. Weichselbaum, W. Lin, Chlorin-based nanoscale metal-organic framework systemically rejects colorectal cancers via synergistic photodynamic therapy and checkpoint blockade immunotherapy, J. Am. Chem. Soc. 138 (2016) 12502–12510.

[16] W. Shan, R. Chen, Q. Zhang, J. Zhao, B. Chen, X. Zhou, S. Ye, S. Bi, L. Nie, L. Ren, Improved stable indocyanine green (ICG)-mediated cancer optotheranostics with naturalized hepatitis B core particles, Adv. Mater. 30 (2018) e1707567.

[17] L. Chen, L. Zhou, C. Wang, Y. Han, Y. Lu, J. Liu, X. Hu, T. Yao, Y. Lin, S. Liang, S. Shi, C. Dong, Tumor-targeted drug and CpG delivery system for phototherapy and docetaxel-enhanced immunotherapy with polarization toward M1-Type macrophages on triple negative breast cancers, Adv. Mater. 31 (2019) e1904997.

[18] K. Ni, T. Luo, G. Lan, A. Culbert, Y. Song, T. Wu, X. Jiang, W. Lin, A nanoscale metal-organic framework to mediate photodynamic therapy and deliver CpG oligodeoxynucleotides to enhance antigen presentation and cancer immunotherapy, Angew. Chem. Int Ed. Engl. 59 (2020) 1108–1112.

[19] S. Wang, J. Campos, M. Gallotta, M. Gong, C. Crain, E. Naik, R.L. Coffman, C. Guiducci, Intratumoral injection of a CpG oligonucleotide reverts resistance to PD-1 blockade by expanding multifunctional CD8+ T cells, Proc. Natl. Acad. Sci. USA 113 (2016) E7240–E7249.

[20] W. Ning, Z. Di, Y. Yu, P. Zeng, C. Di, D. Chen, X. Kong, G. Nie, Y. Zhao, L. Li, Imparting designer biorecognition functionality to metal-organic frameworks by a DNA-mediated surface engineering strategy, Small 14 (2018) e1703812.

[21] Y. Xu, J.J. Moon, Positron emission tomography-guided photodynamic therapy with biodegradable mesoporous silica nanoparticles for personalized cancer immunotherapy, ACS Nano 13 (2019) 12148–12161.

[22] R. Kuai, L.J. Ochyl, K.S. Bahjat, A. Schwendeman, J.J. Moon, Designer vaccine nanodiscs for personalized cancer immunotherapy, Nat. Mater. 16 (2017) 489–496.

[23] B. Liu, F. Hu, J. Zhang, C. Wang, L. Li, A biomimetic coordination nanoplatform for controlled encapsulation and delivery of drug-gene combinations, Angew. Chem. Int Ed. Engl. 58 (2019) 8804–8808.

[24] M. Li, C. Wang, Z. Di, H. Li, J. Zhang, W. Xue, M. Zhao, K. Zhang, Y. Zhao, L. Li, Engineering multifunctional DNA hybrid nanospheres through coordination-driven self-assembly, Angew. Chem. Int Ed. Engl. 58 (2019) 1350–1354.

[25] Y. Zhang, F. Wang, E. Ju, Z. Liu, Z. Chen, J. Ren, X. Qu, Metal-organic-framework-based vaccine platforms for enhanced systemic immune and memory response, Adv. Funct. Mater. 26 (2016) 6454–6461.

[26] Y.P. Jia, K. Shi, F. Yang, J.F. Liao, R.X. Han, L.P. Yuan, Y. Hao, M. Pan, Y. Xiao, Z.Y. Qian, X.W. Wei, Multifunctional nanoparticle loaded injectable thermo-responsive hydrogel as NIR controlled release platform for local photothermal immunotherapy to prevent breast cancer postoperative recurrence and metastases, Adv. Funct. Mater. 30 (2020) 2001059.

[27] J. Pan, Y. Wang, C. Zhang, X. Wang, H. Wang, J. Wang, Y. Yuan, X. Wang, X. Zhang, C. Yu, S.K. Sun, X.P. Yan, Antigen-directed fabrication of a multifunctional nanovaccine with ultrahigh antigen loading efficiency for tumor photothermal immunotherapy, Adv. Mater. 30 (2018) 1704408.

[28] D. Shae, K.W. Becker, P. Christov, D.S. Yun, A.K.R. Lytton-Jean, S. Sevimli, M. Ascano, M. Kelley, D.B. Johnson, J.M. Balko, J.T. Wilson, Endosomolytic polymersomes increase the activity of cyclic dinucleotide STING agonists to enhance cancer immunotherapy, Nat. Nanotechnol. 14 (2019) 269–278.

[29] S. Chattopadhyay, Y.H. Liu, Z.S. Fang, C.L. Lin, J.C. Lin, B.Y. Yao, C.J. Hu, Synthetic immunogenic cell death mediated by intracellular delivery of STING agonist nanoshells enhances anticancer chemo-immunotherapy, Nano Lett. 20 (2020) 2246–2256.

[30] B. Ding, et al., Large-pore mesoporous-silica-coated upconversion nanoparticles as multifunctional immunoadjuvants with ultrahigh photosensitizer and antigen loading efficiency for improved cancer photodynamic immunotherapy, Adv. Mater. 52 (2018) e1802479.

[31] C. He, et al., Core-shell nanoscale coordination polymers combine chemotherapy and photodynamic therapy to potentiate checkpoint blockade cancer immunotherapy, Nat. Commun. 7 (2016) 12499.

[32] Y. Min, et al., Antigen-capturing nanoparticles improve the abscopal effect and cancer immunotherapy, Nat. Nanotechnol. (2017) 877–882.

[33] R. Zhang, Z. Zhu, H. Lv, F. Li, S. Sun, J. Li, C.S. Lee, Immune checkpoint blockade mediated by a small-molecule nanoinhibitor targeting the PD-1/PD-L1 pathway synergizes with photodynamic therapy to elicit antitumor immunity and antimetastatic effects on breast cancer, Small 15 (2019) e1903881.

[34] B.M. Carreno, V. Magrini, M. Becker-Hapak, S. Kaabinejadian, J. Hundal, A.A. Petti, A. Ly, W.R. Lie, W.H. Hildebrand, E.R. Mardis, G.P. Linette, Cancer immunotherapy. A dendritic cell vaccine increases the breadth and diversity of melanoma neoantigen-specific T cells, Science 348 (2015) 803–808.

[35] E. Tran, P.F. Robbins, S.A. Rosenberg, Final common pathway' of human cancer immunotherapy: targeting random somatic mutations, Nat. Immunol. 18 (2017) 255–262.

[36] Q. Chen, L. Xu, C. Liang, C. Wang, R. Peng, Z. Liu, Photothermal therapy with immune-adjuvant nanoparticles together with checkpoint blockade for effective cancer immunotherapy, Nat. Commun. 7 (2016) 13193.

[37] D.M. Klinman, Immunotherapeutic uses of CpG oligodeoxynucleotides, Nat. Rev. Immunol. 4 (2004) 249–258.

[38] W. Guo, C. Guo, N. Zheng, T. Sun, S. Liu, Csx WO3 nanorods coated with polyelectrolyte multilayers as a multifunctional nanomaterial for bimodal imaging-guided photothermal/photodynamic cancer treatment, Adv. Mater. 29 (2017).

[39] F. Chen, Y. Wang, J. Gao, M. Saeed, T. Li, W. Wang, H. Yu, Biomaterials 270 (2021) 120709.

[40] M. Chang, Z. Hou, M. Wang, C. Li, J. Lin, Recent advances in hyperthermia therapy-based synergistic immunotherapy, Adv. Mater. 33 (2021) e2004788.

[41] G. Lan, K. Ni, Z. Xu, S.S. Veroneau, Y. Song, W. Lin, Nanoscale metal−organic framework overcomes hypoxia for photodynamic therapy primed cancer immunotherapy, J. Am. Chem. Soc. 17 (2018) 5670–5673.

[42] G. Lan, K. Ni, R. Xu, K. Lu, Z. Lin, C. Chan, W. Lin, Nanoscale metal−organic layers for deeply penetrating X-rayinduced photodynamic therapy, Angew. Chem., Int. Ed. 40 (2017) 12102–12106.